Cooperative Localization for UAV Systems From the Perspective of Physical Clock Synchronization

Xiaobo Gu, Chengye Zheng, Zeyu Li, Guoxu Zhou, *Member, IEEE*, Haibo Zhou, *Senior Member, IEEE*, and Lian Zhao, *Senior Member, IEEE*

***Abstract*— The positioning accuracy determines the scope of the application of an unmanned aerial vehicle (UAV). In view of the existing UAV cooperative localization methods that normally require prior information and the assistance of external systems, such as the global positioning system (GPS), this study aims to adopt range radios to measure the time-of-arrival (TOA) information among UAVs and then perform clock synchronization and cooperative localization based on ranging measurements. We propose a framework to jointly estimate the clock error and relative distance, adjust the onboard clock, and perform relative positioning. To achieve autonomous clock synchronization and ranging, a practical approach based on peer-to-peer pseudorange measurements is proposed in this study. We modeled the synchronous two-way ranging (STWR) process using a discrete-time state-space model, according to which a linear parameter estimation method and clock steering method are presented. Finally, a closed loop consisting of STWR, parameter estimation, and clock tuning is constructed to improve the ranging accuracy, which leads to improved localization accuracy. Simulation results show that the proposed approach outperforms existing methods and can achieve sub-nanosecond-level time synchronization and meter-level cooperative localization.**

***Index Terms*— Clock steering, cooperative localization, parameter estimation, two-way ranging, unmanned aerial vehicle.**

I. Introduction

A. Background

With the development of integrated electronics and microelectronics engineering, unmanned aerial vehicles (UAV) are being developed for miniaturization and clustering. Compared with existing large single vehicles, such a design has numerous benefits, including a shorter invention period, lower overall cost, flexibility, reconfigurability, and robustness. However, it brings out some problems: One critical issue is achieving accurate clock synchronization and cooperative localization, as these are the preconditions of earth observation, formation flying, and location awareness of ground terminals in an isolated region [1]; the other is avoiding possible collision encounters between the UAV members [2]. Therefore, the system's performance relies on the estimation accuracies of the clock parameters and ranging measurements between UAV members. To satisfy this requirement, UAVs are usually synchronized with the reference clock implemented on the ground station or the global navigation satellite system (GNSS) time [3]. However, these techniques are not applicable to global navigation satellite scenarios with GNSS-denied or strong electromagnetic interference. Moreover, dependence on external systems introduces structural risks for UAVs. For instance, military UAVs would no longer be functional if GNSS satellites or ground stations were destroyed. In addition, frequency syntonization is also paramount to clock synchronization and range. If the frequency and phase of the on-board clock can be steered in real time, it can not only achieve highly accurate clock synchronization for these carrier phase-based ranging techniques but also eliminate the sampling errors originating from the frequency discrepancy.

To achieve clock synchronization, the onboard clock of each UAV must be as accurate and stable as possible. The overall cost, weight, volume, and lifetime of the onboard clock must also be carefully considered. A well-known timekeeping system (TKS), which is designed to produce accurate and precise timing signals for a global positioning system (GPS), consists of atomic clocks and oscillators [4]. However, such a system is not applicable for UAVs, owing to the requirements for low overall cost and low complexity. In addition, the reliance on GPS timing signals limits the scope of the application of UAVs.

Considering these factors, the use of timing signals sent from a member of a self-organized network to steer the local clock has recently become popular. The spread-spectrum communication technique is a common method for building a communication link [5]. It couples communication and synchronization so that the overall cost can be well controlled. By decoding the pseudo-noise (PN) code, the member nodes can communicate with each other and calculate the signal propagation delay by measuring the phase deviation between the reception and local codes. Thus, the relative distance can be obtained based on time-of-arrival (TOA) measurements [6]. Owing to the effect of clock error, an accurate ranging

Manuscript received 15 February 2023; revised 26 June 2023; accepted 13 August 2023. Date of publication 9 October 2023; date of current version 19 December 2023. This work was supported in part by the National Natural Science Foundation of China under Grant 62101138, Grant 62073087, and Grant 62271244; in part by the Guangdong Natural Science Foundation under Grant 2022A1515012573; and in part by the Natural Science Fund for Distinguished Young Scholars of Jiangsu Province under Grant BK20220067. *(Corresponding author: Haibo Zhou.)*

Xiaobo Gu, Chengye Zheng, and Guoxu Zhou are with the School of Automation, and the Key Laboratory of Intelligent Detection and the Internet of Things in Manufacturing, Ministry of Education, Guangdong University of Technology, Guangzhou 510006, China.

Zeyu Li is with the College of Geodesy and Geomatics, Shandong University of Science and Technology, Qingdao 266590, China.

Haibo Zhou is with the School of Electronic Science and Engineering, Nanjing University, Nanjing 210008, China (e-mail: h53zhou@uwaterloo.ca).

Lian Zhao is with the Department of Electrical, Computer, Biomedical Engineering, Toronto Metropolitan University, Toronto, ON M5B 2K3, Canada.

Color versions of one or more figures in this article are available at https://doi.org/10.1109/JSAC.2023.3322797.

Digital Object Identifier 10.1109/JSAC.2023.3322797

measurement must be estimated by decoupling from the pseudorange measurement. Unlike one-way ranging techniques, two-way ranging has been widely implemented in autonomous systems owing to its higher ranging accuracy and capability to decouple clock errors without prior information for immobile networks [7], [8].

In addition, the cooperative localization of a self-organized network can be carried out using range-based positioning approaches, such as multidimensional scaling (MDS) [9], [10] and the extended Kalman filter (EKF) [11], [12], [13]. Similar to the GNSS receivers, a trilateration algorithm can be utilized if more than three anchor nodes are deployed in a network. However, this requirement is impractical for UAV systems and the trilateration algorithm can only localize one node at a time. By contrast, EKF-based methods are typically used to perform multisensor fusion. Positions and velocities must be measured to predict the states of the position parameters. In this study, we addressed the problem of cooperative localization using peer-to-peer ranging measurements. Therefore, MDS-based positioning methods are more feasible in this case. Because the effectiveness of the MDS-based positioning algorithm relies on the ranging accuracy, we can infer that the decoupling error determines the accuracy of time synchronization, ranging, and cooperative positioning. Although solutions based on machine learning techniques have been proposed [14], [15], they are more applicable to indoor positioning than are UAV systems.

In addition, most existing clock synchronization schemes focus on estimating clock offset and clock skew among the system members in a certain network; namely, the discrepancies of the clocks still exist, which we refer to as the 'open loop' method in this paper. The clock signal generated by the open loop inevitably introduces a series of associated errors, such as sampling errors, that cannot be eliminated. However, once the clock error is estimated, a control theory approach can be applied to steer the frequency and phase of the local clock. Subsequently, the adjusted clock generates modified timing signals to perform TOA-based ranging, and the associated errors are eliminated physically. Finally, time and frequency syntonization can be achieved by such a 'closed loop,' which leads to improved ranging accuracy, especially for ranging systems using carrier-smoothed code pseudoranges and carrier phases [16].

B. Previous Works

To realize physical clock synchronization, a common method is to use GNSS receivers for UAV members to receive a 1 pulse per second (PPS) signal and adjust the frequency of the on-board voltage-controlled crystal oscillator (VCXO) [17]. An autoregressive moving average (ARMA) model can be deployed to estimate the clock parameters [18]. However, the accuracy of the synchronization and positioning obtained by this method is limited owing to the GNSS signal structure, and this approach makes the UAVs rely on assistance from external systems. To improve accuracy and autonomy, the reference can be replaced by a system member of the network, which is also similar to GNSS; by broadcasting the designed GNSS-like signals and positions and decoupling the pseudorange measurement at the member node side, network-wide clock synchronization can be achieved [19]. These range ratios have also been applied to UAVs to achieve synchronization, ranging, and relative positioning.

Unlike one-way ranging techniques that require prior information of position and velocity, two-way ranging-based schemes have been presented for years when a GNSS signal or external assistance is not available [20]. The common method is to model the clock using a two-state (clock skew and clock offset) or three-state (clock skew, clock offset, and clock drift) model based on the Taylor series expansion and treat them as parameters to be estimated together with the relative distance. This problem can be solved by constructing an optimization function. In cases where the relative distances are fixed, the problem can be solved by adding or subtracting the forward and reverse links of the same round [21], or by subtracting the forward/reverse links of different rounds [22] to reduce the rank of the column information matrix. These methods are effective in dealing with inaccessible networks with fixed nodes. In addition, the two-way ranging model can be rewritten as a function of virtual clock parameters, which originate from the nonlinear transform of clock skew and clock offset; thus, the clock parameters and relative distance can be jointly estimated in one step, and the estimation accuracy can be improved [23], [24], [25]. Moreover, methods for dealing with mobile nodes have been discussed in [26], [27], and [28], where the anchor nodes were deployed in advance for subsequent signal processing. The scenario in which all nodes are in motion has gained the attention of researchers in recent years. A feasible solution is to make full use of the prior information. For example, in a satellite network, the signal propagation delay can be accurately decoupled owing to the position and velocity information provided by the ephemeris. However, these information is difficult to obtain prior to a UAV swarm. Mobile global least squares (MGLS) [29], which adopts rounds of timing tags for further parameter estimation, is designed to deal with this type of scenario. A polynomial fit approach based on the collected ranging measurements was presented in [30]; however, the problem of synchronization was not considered, and the positioning accuracy was limited. Although some previous studies have proposed estimators of joint clock synchronization and localization, as seen in [20], [31], [32], and [33], the problem of cooperative localization for an inaccessible network in the absence of prior information on the anchor nodes has not been solved. In [34], a joint synchronization and ranging method based on pseudorange measurements was proposed, which required fewer data points than MGLS.

Another problem addressed in this study was clock steering. An overview of the clock-adjustment problem from the viewpoint of control theory was presented in [35]. The clock-steering approach is normally performed periodically and is considered a discrete-time state-space model. In this case, a finite impulse response (FIR) [36] filter and Kalman filter (KF) [37] are applied to adjust the free-running local clocks. Numerous clock-steering algorithms have been proposed for local steering by a one-way reference signal. The problem of clock steering based on two-way ranging has been discussed in [38]; however, the control method was

not optimal. To achieve more accurate clock synchronization in this scenario, a proportional-integral-derivative (PID) controller was presented in [39]. Additionally, the on-board clock can be adjusted not only by the ground station or the GPS 1PPS but also by the reference clock selected from the network members, which could either be a real clock implemented on a member node [38] or a virtual clock elected by the member nodes [40], [41]. These methods focus on the process of control, namely the relationship between the estimated clock errors and the control signal, and are not discussed, especially in the case of a mobile network.

C. Contributions

The contributions of this study are summarized as follows:

- In this paper, we address the problem of achieving time synchronization, frequency syntonization, ranging, and cooperative localization for UAV systems. We derive a novel framework for this scenario, and synchronous two-way ranging (STWR) is adopted to establish the measurement and control network. Only the pseudorange measurements are used for the estimation.
- An improved "ranging, parameter estimation, clock steering, ranging" closed loop is presented, which can maintain the function of physical time synchronization and cooperative localization in the absence of external assistance for an extended period. A Kalman-filter-based approach is proposed within this context.
- As an extension to our previous work [34] and different from the existing approaches, the proposed method can perform time synchronization without prior information due to the proposed relative motion compensation algorithm.

The following notations are used in this study: $\mathbf{I}_m$ is an identity matrix of size $m \times m$ and $\mathbf{0}_{m\times n}$ represents an all-zero matrix of size $m \times n$.

The remainder of this paper is organized as follows: Section II describes the general design of the proposed system. Section III introduces the related ranging and clock models. Section IV describes the detailed process of the proposed method based on the basic models described in Section III. Section V presents the numerical simulation results of the parameter estimation and clock adjustment. Section VI presents conclusions and future work.

II. System Design

A. Closed-Loop Clock Tuning System

To implement the proposed statistical signal processing method for estimating the clock error and relative distance, a closed-loop design was implemented. A general scheme of the clock synchronization loop is presented in Fig.1. The reference/member UAV loads the local pseudorange measurement into a data frame and sends it to the member/reference UAV. Parameter estimation is performed after the pseudorange measurements of the two UAVs have been collected.

The specific functions of each module in the system are as follows:

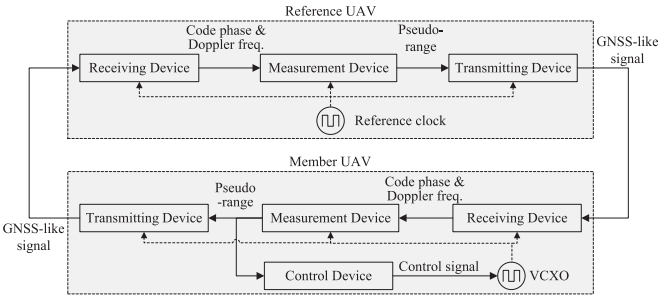

Fig. 1. General scheme of a clock synchronization loop.

Transmitting Device: The transmitting device produces direct-sequence spread spectrum signals for other UAVs. The time and frequency information are concealed within the carrier and pseudocode. The ranging measurement information and the identification number of the UAV are loaded into the data frames of the transmitting signal.

Receiving device: The receiving device receives the signal sent from the transmitting devices of other UAVs. The intermediate frequency is quantized using an analog-to-digital converter. The related ranging data modulated on the pseudocode can be obtained after signal demodulation.

Measurement device: The measurement device performs data recovery, which involves signal acquisition, tracking, and decoding processes. Pseudorange measurements can be obtained from this device.

Control device: The control device is only activated when the UAV is designated as a member node. It is used to generate a clock adjustment signal to control the phase and frequency of the on-board clock. The control signal is calculated using local pseudorange measurements and decoded data.

B. Communication Link Design

The ranging measurements are calculated locally for each UAV. Therefore, a communication network must be constructed to collect ranging measurements. To implement the proposed time synchronization algorithm, a synchronous time division duplex (STDD) structure coupled with code division multiple access (CDMA) was applied. The UAV members simultaneously send GNSS-like signals to each other at the desired time instant; however, a time deviation exists between each pair of communication links at the same time round owing to clock uncertainties. Therefore, the UAV members perform pseudo-synchronous two-way communications. Compared with asynchronous structures, STDD has stricter requirements for time slots [42]. However, it can achieve a more accurate synchronization performance because the relative motion error owing to the asynchronous transmission time can be ignored. In addition, for each communication cycle, each UAV is set to transmit and receive two pseudorange measurements from another visible UAV instead of four timing tags. Such a design can decrease the communication overhead.

III. Related Model

A. Clock Model

In a cooperative mission, the desired events of the system members are normally triggered when a particular time epoch

occurs. Let the accurately known time instants T_n be periodic and $\Delta = T_n - T_{n-1}$ be the uniform sampling rate. Owing to changes in the external environment, aging of internal electronic devices, and random perturbations, a time-varying bias exists between the local on-board clock and the reference clock. The relationship between the reference time and local time can be expressed as

$$G_i(n) = T_n + \delta_i(n), \tag{1}$$

where $G_i(n)$ and $\delta_i(n)$ denote the global time of node i and the clock offset between the reference and node i in the n^{th} communication cycle, respectively.

The recursive state evolution model that accounts for the clock behavior at successive synchronization instants can be written in matrix form as follows:

$$\begin{bmatrix} \delta_i(n+1) \\ \omega_i(n+1) \end{bmatrix} = \begin{bmatrix} 1 & \Delta \\ 0 & 1 \end{bmatrix} \begin{bmatrix} \delta_i(n) \\ \omega_i(n) \end{bmatrix} + \begin{bmatrix} \varepsilon_\delta(n) \\ \varepsilon_\omega(n) \end{bmatrix}, \tag{2}$$

where $\delta_i(n)$ and $\omega_i(n)$ represent the clock offset and clock skew at the nth signal transaction, respectively. The stochastic processes ε_δ and ε_ω describe the state noise, which is an independent white Gaussian noise with zero mean. The covariance matrix of the noise components is given by [43]

$$\mathbf{\Xi}_\varepsilon = \begin{bmatrix} q_1\Delta + q_2\Delta^3/3 & q_2\Delta^2/2 \\ q_2\Delta^2/2 & q_2\Delta \end{bmatrix}, \tag{3}$$

where q_1 and q_2 denote the process noise parameters of ε_δ and ε_ω, also called white frequency model (WFM) noise and random walk frequency model (RWFM) noise, respectively.

In general, the metric for characterizing the stability of a clock is the Allan Variance, which is given by

$$\sigma_a^2(\tau) = \frac{1}{2}E\left[\left(f(n)^{(l)} - f(n-l)^{(l)}\right)^2\right], \tag{4}$$

where

$$f(n)^{(l)} = \frac{1}{l}\sum_{m=0}^{l-1} f(n-m), \tag{5}$$

$$f(n) = (\delta_n - \delta_{n-1})/\Delta, \tag{6}$$

where $\tau = l \cdot \Delta$. The relationship between the diffusion coefficients and the Allan Variance is expressed as

$$\sigma_a^2(\tau) = \frac{q_1}{\tau} + \frac{q_2\tau}{3}. \tag{7}$$

Related theoretical analyses and deduction processes are presented in [43]. Therefore, noise characterization of the clock can be conducted once the Allan variance is known.

B. Ranging Model

To estimate UAV clock errors remotely, the basic premise is to build a two-way communication link to exchange information; that is, a communication network among UAV members is required. CDMA is used to establish a communication network. According to this spread-spectrum communication technique, clock errors can be calculated indirectly by pseudorange measurements obtained from the PN code.

Inspired by [42], the STDD is adopted in this study to effectively eliminate the "transceiver isolation" issue in the full-duplex system and reduce its complexity. It is noted that the UAVs do not transmit signals to others at the same global time instant owing to clock errors, although they are appointed to transmit signals at the same local time epoch.

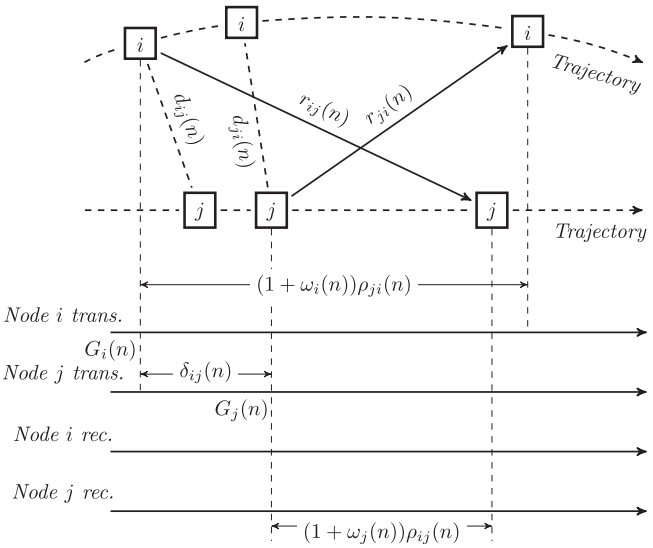

Fig. 2. The schematic of STWR between node i and node j at the k^{th} communication cycle.

A schematic of the STDD based two-way ranging, which we call STWR in this study, is shown in Fig.2.

The principle of STWR is as follows: For the n^{th} round of transmission, both nodes transmit the ranging signal to each other at their local time instant T_n. A transmission delay occurs between the two nodes owing to the clock error $\delta_{ij}(n) = \delta_j(n) - \delta_i(n)$, hence their global transmitting time instants are $G_i(n)$ and $G_j(n) = G_i(n) + \delta_{ij}(n)$ respectively; $d_{ij}(n)\,\{d_{ji}(n)\}$ denotes the relative Euclidean distance at time instant $G_i(n)\,\{G_j(n)\}$, whereas $r_{ij}(n)\,\{r_{ji}(n)\}$ denotes the signal transmission distance from $i\,\{j\}$ to $j\,\{i\}$ at the n^{th} communication cycle; $\rho_{ij}(n)\,\{\rho_{ji}(n)\}$ denotes the pseudorange measurement obtained from node $j\,\{i\}$ at the n^{th} communication cycle; and c denotes the speed of light.

The nth round of STWR can be modelled as

$$(1+\omega_j(n))\rho_{ij}(n)c^{-1} = \chi_{ij}(n) - \delta_{ij}(n) + \alpha_{ij}(n), \tag{8}$$

$$(1+\omega_i(n))\rho_{ji}(n)c^{-1} = \chi_{ji}(n) + \delta_{ij}(n) + \alpha_{ji}(n), \tag{9}$$

where $\chi_{ij}(n) \triangleq \chi_{ij}(G_i(n)) = r_{ij}(n)c^{-1}$ $\{\chi_{ji}(n) \triangleq \chi_{ji}(G_j(n)) = r_{ji}(n)c^{-1}\}$ are the signal transmission times from node $i\{j\}$ to node $j\{i\}$ at the n^{th} communication cycle; α_{ij}^k and α_{ji}^k denote the aggregated noises that originate from the space disturbance, measurement, clock uncertainty, and the change in the outside environment, which is assumed to be described by Gaussian variables with zero mean and variance σ^2.

IV. Proposed Estimator

A. Relative Motion Modelling

If the positions of nodes i and j are fixed, then $\chi_{ij}(n) = \chi_{ji}(n) = d_{ij}(n)c^{-1} = d_{ji}(n)c^{-1}$; numerous clock synchronization and ranging algorithms have been proposed in

this case. However, if the two nodes are in motion and the transaction times $\chi_{ij}(n)$ and $\chi_{ji}(n)$ change with the elapsed time, which yields $\chi_{ij}(n) \neq \chi_{ji}(n)$, the conventional two-way ranging technique would no longer be feasible in this case. Additionally, the relative distance $d_{ij}(n)$ is not equal to the transmission distance $r_{ij}(n)$. Therefore, $d_{ij}(n)$ and $d_{ji}(n)$ must be modeled.

The relationship between $d_{ij}(n)$ and $r_{ij}(n)$ can be expressed as [42]

$$d_{ij}(n)c^{-1} = \chi_{ij}(n) + \chi_{ij}(n) \cdot \overline{v}^{j}_{LOS} \cdot c^{-1}, \tag{10}$$

where $\overline{v}^{j}_{LOS}$ denotes the average line-of-sight velocity in $\chi_{ij}(n)$. Because the line-of-sight velocity, which is a velocity component of a UAV, is much smaller than the speed of light, the approximation $d_{ij}(n)c^{-1} \approx \chi_{ij}(n)$ can be obtained in this study.

The transaction signal delays $\chi_{ij}(n)$ and $\chi_{ji}(n)$ are functions of n, and can be modeled by Taylor-series as follows:

$$\begin{aligned}\chi_{ij}(n) &\triangleq \chi_{ij}(G_i(n)) \\ &= \beta_{ij,0} + \beta_{ij,1}G_i(n) + \cdots + \beta_{ij,K}G_i(n)^K, \end{aligned}\tag{11}$$

$$\begin{aligned}\chi_{ji}(n) &\triangleq \chi_{ji}(G_j(n)) \\ &= \beta_{ji,0} + \beta_{ji,1}G_j(n) + \cdots + \beta_{ji,K}G_j(n)^K, \end{aligned}\tag{12}$$

where K denotes the order of the Taylor expansion and $\left[\beta_{ij,0}, \beta_{ij,1}, \ldots, \beta_{ij,K}\right] \in \mathbb{R}^{(K+1)\times 1}$ and $\left[\beta_{ji,0}, \beta_{ji,1}, \ldots, \beta_{ji,K}\right] \in \mathbb{R}^{(K+1)\times 1}$ are the coefficients of the polynomial. Such a model is also feasible for various scenarios of the anchor nodes; namely, $\beta_{ij,0} = \beta_{ji,0}$ represents the relative distance, and $\beta_{ij,k} = \beta_{ji,k} = 0$, where $k = \{1, \ldots, K\}$.

Without a loss of generality, let node i be the reference, which leads to $\delta_i = 0$ and $\omega_i = 0$. Substituting the equation $\delta_i = 0$ into (1), we obtain $T_n = G_i(n)$. Therefore, (11) can be rewritten as

$$\chi_{ij}(n) \triangleq \chi_{ij}(T_n) = \beta_{ij,0} + \beta_{ij,1}T_n + \cdots + \beta_{ij,K}T_n^K, \tag{13}$$

For simplicity, for $\chi_{ji}(n)$, the following assumption can be made.

$$\chi_{ji}(n) \triangleq \chi_{ji}(G_j(n)) \approx \chi_{ij}(G_j(n) + \chi_{ji}(n)) \tag{14}$$

This is because the signal transmission times are usually much smaller than the time tags; thus, the requirement of the full column rank can be met and the calculation can be simplified. Figure 2 shows that

$$\begin{aligned} G_j(n) + \chi_{ji}(n) &= G_i(n) + (1 + \omega_i(n))\rho_{ji}(n)c^{-1} \\ &= T_n + (1 + \omega_i(n))\rho_{ji}(n)c^{-1} \\ &\approx T_n + \rho_{ji}(n)c^{-1}. \end{aligned}\tag{15}$$

Substituting (14) and (15) into (12), we have [See (16), as shown at the bottom of the next page.]

Substituting the constraint of the reference node $\delta_i = 0$, $\omega_i = 0$ and the approximation equations (13) and (16) back into (8) and (9), we obtain [See (17) and (18), as shown at the bottom of the next page.]

Two critical assumptions have been made to deal with the problem of few observations. The first is to represent $\chi_{ij}(n)$ and $\chi_{ji}(n)$ with a unified function. Therefore, we can infer that velocity and moving direction play important roles in the performance of the proposed estimator. For instance, when nodes i and j move at the same speed along the positive directions of the x and y axes, respectively, the proposed estimator achieves better performance. This is because in this case, $\chi_{ij}(t) = \chi_{ji}(t)$. Another assumption is that $G_j(n) \approx G_j(n) + \chi ji(n)$ in (14) because $G_j(n) \gg \chi ji(n)$. The premise of this assumption is that the relative distance between the UAVs is normally small; therefore, the signal transmission delay is small. Based on this approximation, (15) and (16) can be derived as the sum of the transmission delay and transmission time instances of node j, which is equal to the reception delay of node i.

B. Network-Wide Estimator

Based on the discussions above, we can extend the proposed framework from pairwise mode to network-wide mode. Let N be the number of UAVs, and node 1 be the reference node. If each UAV in the system can communicate and range with other UAVs, we can infer that the number of unknown clock parameters is $2N - 2$ and that of communication links is $\Psi = \binom{N}{2}$. Hence, the number of ranging parameters is $\psi = (K + 1) \cdot \Psi$. We propose a discrete clock-steering model coupled with a ranging model, which can be represented by a time-varying linear state-space model with respect to the state and observation equations given by

$$\mathbf{X}(n) = \mathbf{L}\mathbf{X}(n-1) + \mathbf{B}\mathbf{\Lambda}(n) + \boldsymbol{\varepsilon}(n), \tag{19}$$

where $\mathbf{X}(n) = [\boldsymbol{\beta}\ \boldsymbol{\delta}(n)\ \boldsymbol{\omega}(n)]^T \in \mathbb{R}^{(\psi+2N-2)\times 1}$ denotes the unknown clock and ranging parameters, $\boldsymbol{\beta} = \left[\boldsymbol{\beta}_{12}\ \ldots \boldsymbol{\beta}_{1N}\ \boldsymbol{\beta}_{23} \ldots \boldsymbol{\beta}_{2N} \ldots \boldsymbol{\beta}_{(N-1)(N)}\right]^T \in \mathbb{R}^{\psi\times 1}$, with sub-vector $\boldsymbol{\beta}_{ij} = [\beta_{ij,0}\ \beta_{ij,1} \ldots \beta_{ij,K}] \in \mathbb{R}^{1\times(K+1)}$; $\boldsymbol{\delta} = [\delta_2(n) \ldots \delta_N(n)]^T \in \mathbb{R}^{(N-1)\times 1}$,$\boldsymbol{\omega} = [\omega_2(n) \ldots \omega_N(n)]^T \in \mathbb{R}^{(N-1)\times 1}$, and $\mathbf{\Lambda}(n) = [\mathbf{0}_\psi\ \boldsymbol{\mu}_{\boldsymbol{\delta}}(n)\ \boldsymbol{\mu}_{\boldsymbol{\omega}}(n)]^T \in \mathbb{R}^{(\psi+2N-2)\times 1}$ denotes the input control vector, $\mathbf{0}_\psi = [0\ 0\ \ldots\ 0]^T \in \mathbb{R}^{\psi\times 1}$; $\mathbf{L}$ and $\mathbf{B}$ are the coefficient matrices, expressed by

$$\mathbf{L} = \begin{bmatrix} \mathbf{I}_\psi & \mathbf{0}_{\psi\times(N-1)} & \mathbf{0}_{\psi\times(N-1)} \\ \mathbf{0}_{(N-1)\times\psi} & \mathbf{I}_{N-1} & \Delta \cdot \mathbf{I}_{N-1} \\ \mathbf{0}_{(N-1)\times\psi} & \mathbf{0}_{(N-1)\times(N-1)} & \mathbf{I}_{N-1} \end{bmatrix}, \tag{20}$$

$$\mathbf{B} = \begin{bmatrix} \mathbf{0}_{(\psi+N-1)\times(\psi+N-1)} & \mathbf{0}_{(\psi+N-1)\times(N-1)} \\ \mathbf{0}_{(N-1)\times(\psi+N-1)} & -\mathbf{I}_{N-1} \end{bmatrix}, \tag{21}$$

As the ranging parameters $\boldsymbol{\beta}$ are considered constants within the communication cycles, we let $\boldsymbol{\varepsilon}(n) = [\mathbf{0}_{\psi\times 1}, \boldsymbol{\varepsilon}_\omega(n), \boldsymbol{\varepsilon}_\delta(n)]$, where $\boldsymbol{\varepsilon}_\omega(n)$ and $\boldsymbol{\varepsilon}_\delta(n)$ denote the corresponding noise components of RWPM and RWFM, respectively.

In addition, the observation matrix can be obtained by stacking (17) and (18) into a matrix form, which yields

$$\mathbf{Z}(n) = \mathbf{C}(n)\mathbf{X}(n) + \mathbf{v}(n), \tag{22}$$

where $\mathbf{Z}(n) = c^{-1}\left[\boldsymbol{\rho}_{12}(n) \ldots \boldsymbol{\rho}_{1N}(n) \ldots \boldsymbol{\rho}_{(N)(N-1)}(n)\right]^T \in \mathbb{R}^{2\Psi\times 1}$, with sub-vectors $\boldsymbol{\rho}_{ij}(n) = [\rho_{ij}(n)\ \rho_{ji}(n)]$,

$\mathbf{C}(n) = [\mathbf{\Omega}(n)\ \mathbf{T}(n)] \in \mathbb{R}^{2\Psi\times(\psi+2N-2)}$. The sub-matrices $\mathbf{\Omega}(n)$ and $\mathbf{T}(n)$ are expressed by (23) and (24), as shown at the bottom of the page.

Based on the state equation (19) and the observation equation (22), a practical linear Kalman filter can be summarized as

Prediction:

$$\hat{\mathbf{X}}(n \mid n-1) = \mathbf{L}\hat{\mathbf{X}}(n-1 \mid n-1) + \mathbf{B}(n \mid n-1)\hat{\mathbf{\Lambda}}(n-1), \tag{25}$$

$$\mathbf{H}(n \mid n-1) = \mathbf{L}\mathbf{H}(n-1 \mid n-1)\mathbf{L}^T + \mathbf{Q}, \tag{26}$$

Update:

$$\mathbf{K}(n) = \mathbf{H}(n \mid n-1)\mathbf{C}(n)^T \left[\mathbf{C}(n)\mathbf{H}(n \mid n-1)\mathbf{C}(n)^T + \mathbf{R}\right]^{-1}, \tag{27}$$

$$\hat{\mathbf{X}}(n \mid n) = \hat{\mathbf{X}}(n \mid n-1) + \mathbf{K}(n)\left[\mathbf{Z}(n) - P\mathbf{C}(n)\hat{\mathbf{X}}(n \mid n-1)\right], \tag{28}$$

$$\mathbf{H}(n \mid n) = \left[\mathbf{I}_{\psi+2N-2} - \mathbf{K}(n)\mathbf{C}(n)\right]\mathbf{H}(n \mid n-1), \tag{29}$$

where $\mathbf{H}$ is the mean square error matrix of the posteriori estimation error of the state variable; $\mathbf{K}$ denotes the gain matrix of the Kalman filter; and $\mathbf{Q} = E(\boldsymbol{\varepsilon}(n)\boldsymbol{\varepsilon}(n)^T) \in \mathbb{R}^{(\psi+2N-2)\times(\psi+2N-2)}$ and $\mathbf{R} = E(\mathbf{v}(n)\mathbf{v}(n)^T) \in \mathbb{R}^{2\Psi\times 2\Psi}$ are the noise covariance matrices of the state equation and observation equation, respectively.

The ranging parameter $\boldsymbol{\beta}$ and clock parameters $[\boldsymbol{\delta}(n), \boldsymbol{\omega}(n)]$ are assumed to be independent. In contrast, the clock skew and offset are not independent, as discussed in Section III-A, and the related covariance matrix is represented by (3). Therefore, the covariance matrix $\mathbf{Q}(n)$ can be modeled as

$$\mathbf{Q} = \begin{bmatrix} \mathbf{0}_{\psi\times\psi} & \mathbf{0}_{\psi\times(N-1)} & \mathbf{0}_{\psi\times(N-1)} \\ \mathbf{0}_{(N-1)\times\psi} & (q_1\Delta + q_2\Delta^3/3)\mathbf{I}_{N-1} & (q_2\Delta^2/2)\mathbf{I}_{N-1} \\ \mathbf{0}_{(N-1)\times\psi} & (q_2\Delta^2/2)\mathbf{I}_{N-1} & (q_2\Delta)\mathbf{I}_{N-1} \end{bmatrix}. \tag{30}$$

As specified in [42] and [44], the observation noise of a communication link contains ranging measurements, unidirectional combined hardware delays, and space disturbances. We assumed that these error sources were calibrated in advance, and the $\mathbf{v}(n)$ in observation equations (17) and (18) denotes the combined residual noise components. As the forward and reverse links are independent, the covariance matrix of the observation equation (22) can be expressed as

$$\mathbf{R} = \sigma^2\mathbf{I}_{2\Psi}. \tag{31}$$

An important issue with the STDD is that the signals must be transmitted and received at the same local time. Although the signals are not transmitted simultaneously owing to clock errors, they still require good orthogonality of the PN codes. A feasible solution is to apply a frequency-division duplex (FDD) along with STDD when the number of UAVs is small. In addition, if the relative distance is sufficiently long, we can only use STDD to solve this problem. In other words, we can design different signal reception timeslots for each member

$$\chi_{ji}(n) = \beta_{ij,0} + \beta_{ij,1}(T_n + \rho_{ji}(n)c^{-1}) + \beta_{ij,2}(T_n + \rho_{ji}(n)c^{-1})^2 + \cdots + \beta_{ij,K}(T_n + \rho_{ji}(n)c^{-1})^K. \tag{16}$$

$$\rho_{ij}(n)c^{-1} = \beta_{ij,0} + T_n\beta_{ij,1} + \cdots + T_n^K\beta_{ij,K} - \rho_{ij}(n)c^{-1}\omega_j(n) - \delta_j(n) + \delta_i(n) + \alpha_{ij}(n), \tag{17}$$

$$\rho_{ji}(n)c^{-1} = \beta_{ij,0} + (T_n + \rho_{ji}(n)c^{-1})\beta_{ij,1} + \cdots + (T_n + \rho_{ji}(n)c^{-1})^K\beta_{ij,K} + \delta_j(n) - \delta_i(n) + \alpha_{ji}(n). \tag{18}$$

$$\mathbf{\Omega}(n) = \begin{bmatrix} 1 & T_n & \cdots & T_n^K & \cdots & 0 & 0 & \cdots & 0 \\ 1 & T_n + \rho_{21}(n)c^{-1} & \cdots & (T_n + \rho_{21}(n)c^{-1})^K & \cdots & 0 & 0 & \cdots & 0 \\ \vdots & \vdots & \ddots & \vdots & \ddots & \vdots & \vdots & \ddots & \vdots \\ 0 & 0 & \cdots & 0 & \cdots & 1 & T_n & \cdots & T_n^K \\ 0 & 0 & \cdots & 0 & \cdots & 1 & T_n + \rho_{(N)(N-1)}(n)c^{-1} & \cdots & (T_n + \rho_{(N)(N-1)}(n)c^{-1})^K \end{bmatrix}, \tag{23}$$

$$\mathbf{T}(n) = \begin{array}{r} \text{node } 1 \to \text{node } 2 \\ \text{node } 2 \to \text{node } 1 \\ \vdots \\ \text{node } 1 \to \text{node } N \\ \text{node } N \to \text{node } 1 \\ \text{node } 2 \to \text{node } 3 \\ \text{node } 3 \to \text{node } 2 \\ \vdots \\ \text{node } 2 \to \text{node } N \\ \text{node } N \to \text{node } 2 \\ \vdots \\ \text{node } N-1 \to \text{node } N \\ \text{node } N \to \text{node } N-1 \end{array} \begin{bmatrix} -1 & 0 & \cdots & 0 & 0 & \mathbf{0}_{1\times(N-1)} \\ 1 & 0 & \cdots & 0 & 0 & \mathbf{0}_{1\times(N-1)} \\ \vdots & \vdots & \ddots & \vdots & \vdots & \vdots \\ 0 & 0 & \cdots & 0 & -1 & \mathbf{0}_{1\times(N-1)} \\ 0 & 0 & \cdots & 0 & 1 & \mathbf{0}_{1\times(N-1)} \\ 1 & -1 & \cdots & 0 & 0 & \mathbf{0}_{1\times(N-1)} \\ -1 & 1 & \cdots & 0 & 0 & \mathbf{0}_{1\times(N-1)} \\ \vdots & \vdots & \ddots & \vdots & \vdots & \vdots \\ 1 & 0 & \cdots & 0 & -1 & \mathbf{0}_{1\times(N-1)} \\ -1 & 0 & \cdots & 0 & 1 & \mathbf{0}_{1\times(N-1)} \\ \vdots & \vdots & \ddots & \vdots & \vdots & \vdots \\ 0 & 0 & \cdots & 1 & -1 & \mathbf{0}_{1\times(N-1)} \\ 0 & 0 & \cdots & -1 & 1 & \mathbf{0}_{1\times(N-1)} \end{bmatrix}. \tag{24}$$

as long as the sum of all the signal reception timeslots is shorter than the signal propagation time. As can be inferred, the proposed estimator is also applicable to conventional time-division multiple access (TDMA) networks. Although the estimation accuracy is degraded, the performance relies on the velocities, positions, and numbers of UAVs, indicating that the proposed estimator is still feasible in some cases.

C. Input Signal

Once the clock offset and clock skew are jointly estimated according to the clock synchronization protocol, an input signal $\mathbf{\Lambda}(n)$ can be generated to control the frequency and phase of the member clock.

To control the VCXO and achieve time synchronization and frequency syntonization, an input control signal must be generated to construct a closed loop. This is normally set to the opposite of the estimated clock skew $\hat{\omega}(n)$ and clock offset $\hat{\delta}(n)$ [38], [45]. However, this approach is not feasible for our proposed model because it takes time to accomplish two-way communication to collect ranging information; namely, the n^{th} round of ranging information calculated at the neighbor node can only be obtained at the $(n+1)^{th}$ round of two-way communication. Furthermore, clock adjustment must be performed at the $(n+2)^{th}$ time slot. Therefore, the clock offset accumulated during the two time slots must be considered when generating a control signal. The clock offset of the $(n+2)^{th}$ time slot can be estimated using a linear Kalman filter.

The clock skew can be adjusted because the frequency of the VCXO is adjustable. In addition, phase correction can be performed by changing the phase-control word (PCW) of the clock. When the estimated clock offset is much greater than the limited pulling rate of the VCXO, a long time is required for the control loop to converge. To solve this problem, we set a phase control signal $\delta_{threshold}$ to optimize the clock adjustment process. When the estimated clock offset $\hat{\delta}(n+2)$ is greater than $\delta_{threshold}$, we set the phase adjustment signal $\mu_\delta(n+2)$ by changing the initial count value of the next round of PCW as follows:

$$\mu_\delta(n+2) = \frac{\hat{\delta}(n+2) \cdot H_{max}}{2\pi}, \tag{32}$$

where H_{max} is the maximum count value of PCW. Otherwise, the phase control signal $\mu_\delta(n+2) = 0$, and the frequency adjustment procedure begins. Notably, changing the phase of the local clock may lead to a loss of locks in the tracking loop. However, because each UAV is required to reacquire ranging signals in each communication cycle, this concern can be ignored in this STDD-based network.

The frequency-adjustment signal is generated by

$$\mu_\omega(n+2) = g(\hat{\delta}(n+2), \hat{\omega}(n+2)), \tag{33}$$

where the function $g(\bullet)$ is a 3^{rd} order PLL coupled with a 2^{nd} order FLL. Moreover, $\mu_\omega(n+2)$ should be set in the proper range $[0, \mu_{\omega max}]$ to prevent the clock from experiencing short-term stability deterioration. For instance, if the short-term stability of the VCXO is $\sigma_{osc} = 1 \times 10^{-11}$ per second

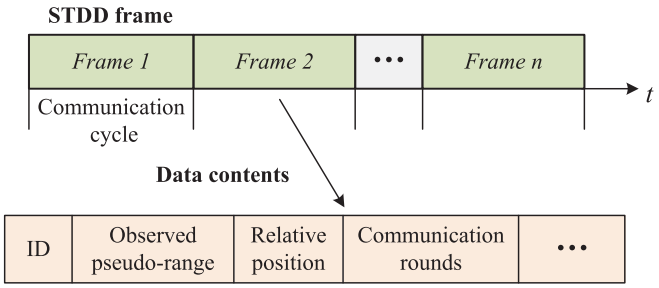

Fig. 3. The data frame transmitted by the proposed STDD frame.

and we assume that the stability after clock adjustment is no greater than $1.05\sigma_{osc}$, then

$$1.05\sigma_{osc} = \sqrt{\sigma_{osc}^2 + \mu_{\omega max}^2}, \tag{34}$$

Therefore, $\mu_{\omega max} = 3.2 \times 10^{-12}$.

To accelerate the synchronization rate and keep the clock adjustment loop stable, we propose a method to generate the input signal $\mathbf{\Lambda}(n)$, which can adjust clock offset and clock skew simultaneously. A schematic is shown in Fig. 4.

Based on the discussions above, a novel pseudo-synchronous scheduling scheme is proposed in this paper that can measure and exchange the ranging information, predict the clock error, and generate the control signal. The process details are summarized as follows:

Step 1: Pseudorange Measurement: For the n^{th} round of two-way ranging, nodes i and j transmit the ranging signals to each other at local time T_n. The pseudocode ranging measurements $\rho_{ij}(n)$ and $\rho_{ji}(n)$ can be obtained after spread-spectrum signal processing, including acquisition, tracking, and ranging. Each node then loads the observed $\rho_{ij}(n)$ and $\rho_{ji}(n)$ into the data frame, which is then transmitted in the next round of two-way ranging. $\rho_{ij}(n)$ and $\rho_{ji}(n)$ are also locally stored.

Step 2: Data Exchange: In the $(n+1)^{th}$ round of two-way ranging, each node transmits the ranging signal to the others and obtains local pseudo-code ranging measurements $\rho_{ij}(n+1)$ and $\rho_{ji}(n+1)$. On the other hand, the measurements $\rho_{ij}(n)$ can be obtained at node i after data frame demodulation, and vice versa. Therefore, both nodes collect the n^{th} round of two-way ranging measurements, $\rho_{ij}(n)$ and $\rho_{ji}(n)$, at this stage.

Step 3: Clock Error Prediction: Using (17) and (18), the relative clock skew $\hat{\omega}_j(n)$ and clock offset $\hat{\delta}_j(n)$ between the two nodes can be estimated. However, the clock error parameters used to generate the input control signal are $\hat{\omega}_j(n+2)$ and $\hat{\delta}_j(n+2)$ because the signal control time is set to start at the $(n+2)^{th}$ round of two-way ranging. A linear estimator based on (19) is used for this prediction.

Step 4: Clock Adjustment: At the $(n+2)^{th}$ time slot, the member node starts to adjust its local clock. The control signal is generated using a 3^{rd} order phase lock loop coupled with a 2^{nd} order frequency lock loop.

Once the ranging parameters are estimated, the relative distance can be approximated using (13) and (16). These pairwise distances simultaneously construct a Euclidean distance matrix (EDM), which is the input for cooperative localization using MDS-based algorithms. Fig. 3 shows the data frame of

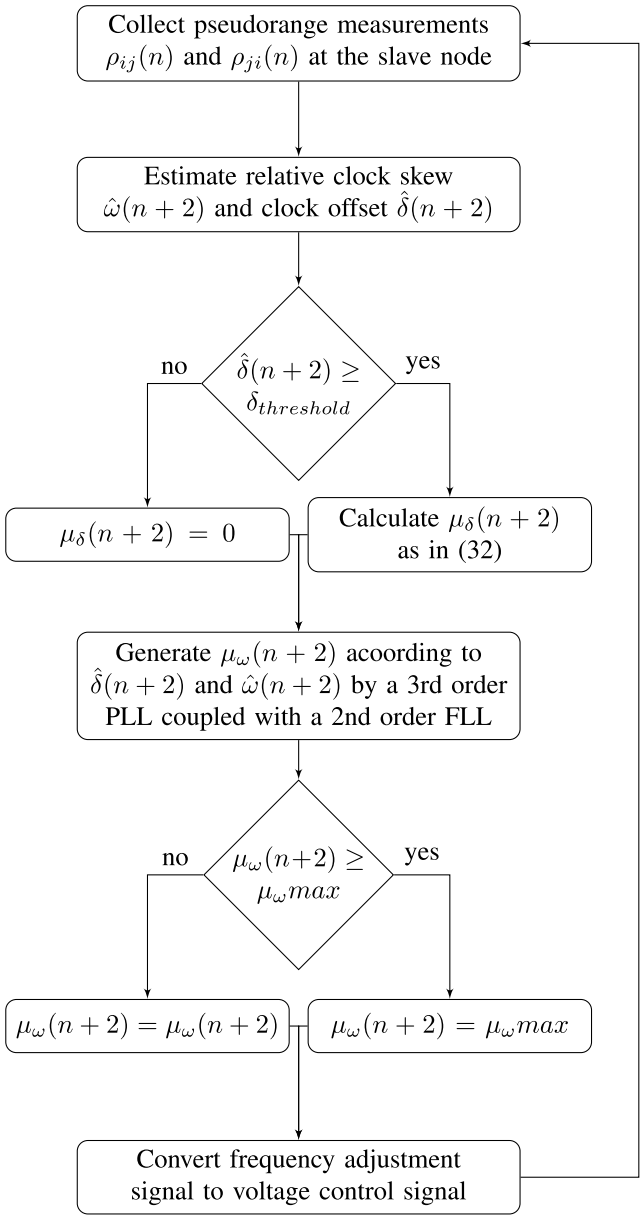

Fig. 4. Generic schematic showing member blocks and processing functions.

the proposed STDD scheduling scheme. Each frame contains information on the identification number, locally observed pseudorange measurements, estimated relative position, and current communication rounds. MDS only provides the position in a relative coordinate frame; thus, the position in a reference coordinate frame is required for coordinate mapping. The estimated position obtained from node 1 can be defined as the reference coordinate frame to solve this problem. For the positioning of subsequent communication cycles, the velocity information obtained from the carrier-phase tracking loop can be used to achieve continuous cooperative localization.

D. Complexity Comparisons

By analyzing the calculation process presented in (25)–(29), we can infer that the proposed estimator, in the absence of clock steering, takes the complexity order

Algorithm 1 Physical Time Synchronization, Ranging, and Cooperative Localization Strategy

Require: $\hat{\mathbf{X}}_i(0|0)$, $\mathbf{H}_i(0|0)$, $\mathbf{Q}$, $\mathbf{R}$

for $n = 0, 1, 2, \ldots,$ Do **do**
  $n = n + 1$
  Input: $\boldsymbol{\rho}_{12}(n), \ldots, \boldsymbol{\rho}_{1N}(n), \ldots, \boldsymbol{\rho}_{(N)(N-1)}(n)$
  Update: $\hat{\mathbf{X}}(n \mid n)$ as in (25) - (29)
  if $n > 2$ **then**
    Update: $\hat{\mathbf{\Lambda}}(n)$ as in Fig. 4
  end if
  Update: $d_{ij}(n)$ and $d_{ji}(n)$ as in (10) - (12)
  Construct EDM of the n^{th} communication cycle
  Perform cooperative localization via MDS
end for

$\mathcal{O}\left((\psi + 2N - 2)^3\right)$, whereas the complexity order of conventional two-way ranging is $\mathcal{O}\left(8\psi^3\right)$. According to the relationship between ψ and N, we can infer that both the two complexity terms belongs to the same complexity class. However, there are two main differences between the proposed estimator and conventional two-way ranging approach. For each round of communication, the information transmitted between the nodes is a pair of pseudorange measurements, whereas the conventional two-way ranging approach requires four time stamps. In addition, conventional two-way ranging must reduce the dimensions of the parameters by the process of addition (subtraction) of the forward and reverse links before estimating the parameters to meet the requirement of full column rank. In addition, for low complexity, some existing two-way ranging methods [21], [23], [25] estimate the virtual clock parameters to linearize the estimator, which leads to an extra nonlinear transformation process to transform these virtual parameters into realistic parameters. In contrast, the proposed estimator can jointly estimate the clock and range parameters in one step.

V. Simulations

A software platform based on MATLAB was set up to test the proposed method. We considered a scenario with $N = 5$ UAVs in a 3-D space where UAVs remained visible to each other during the entire simulation time. Each pair of UAV members was assumed to be visible during the simulation. Without a loss of generality, node 1 was selected as the reference node. We let the pseudorange measurement uncertainty $\sigma = 1 \times 10^{-7}$s, clock uncertainties $q_1 = 1 \times 10^{-12}$s and $q_2 = 1 \times 10^{-10}$, initial state of KF $\hat{\mathbf{X}}(0|0) = \mathbf{0}_{(\psi+2N-2)\times 1}$, $\hat{\mathbf{H}}(0|0) = \mathbf{I}_{(\psi+2N-2)}$, and the initial accumulated clock offset and clock skew be randomly selected in the ranges $[-0.001, 0.001]$s and $\left[1 \times 10^{-9}, 1 \times 10^{-8}\right]$. The loop bandwidth cannot be an arbitrarily small value; otherwise, the dynamic stress tolerance may be exceeded. Therefore, the bandwidths of the PLL and FLL were set to 0.35 and 0.06 Hz, respectively. The damping parameter was $\frac{1}{\sqrt{2}}$. Parameter selection for each order can be found in [16]. The global scalar performance parameter, root average mean square error (RAMSE), was adopted to evaluate the performance of the

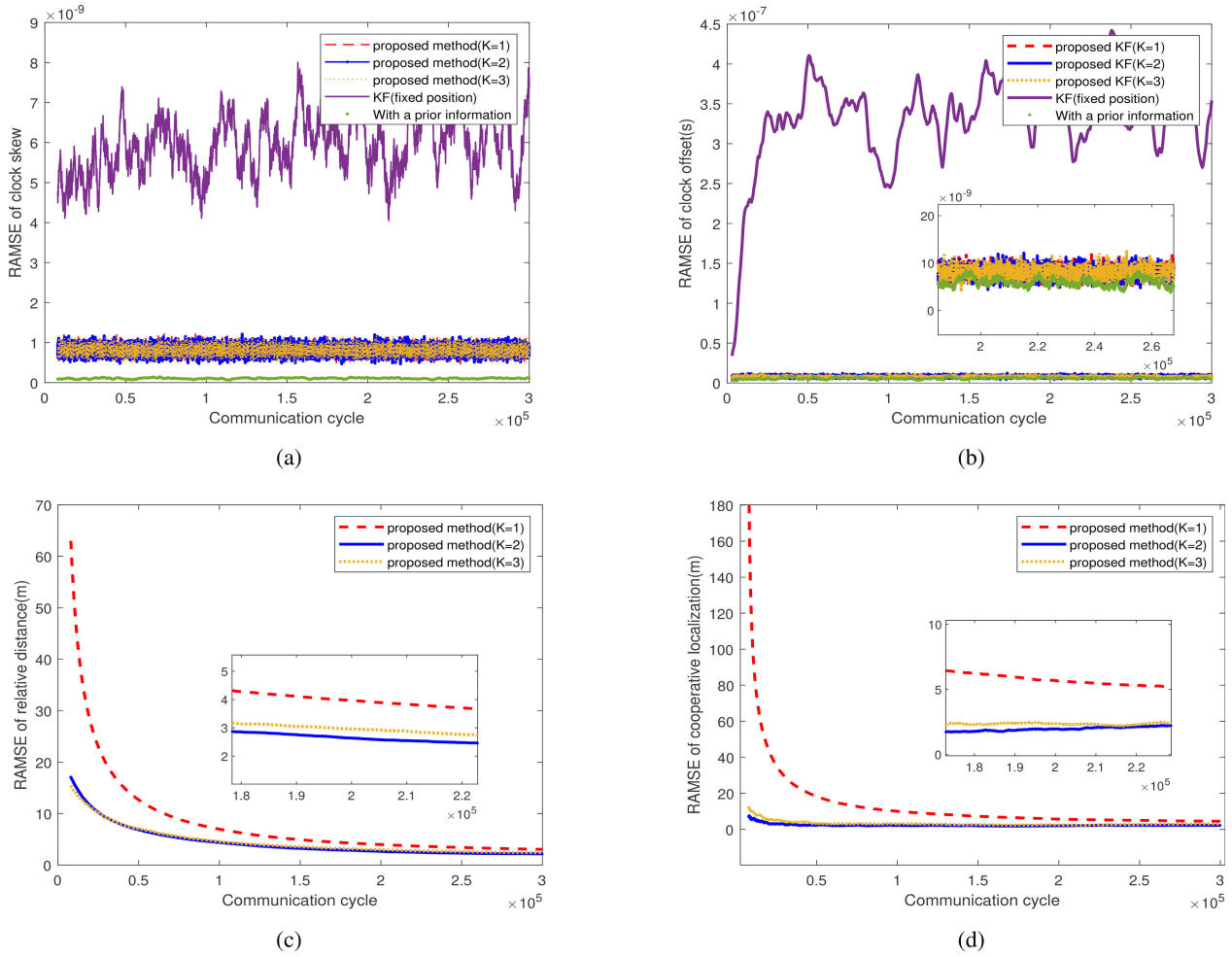

Fig. 5. RAMSEs for clock skew (a), clock offset (b), relative distance (c), and cooperative localization (d) with respect to the communication cycles in the scenario with initial positions $\mathbf{P}_2$ and velocities $\dot{\mathbf{P}}_2$.

existing methods and is expressed as

$$\mathrm{RAMSE}(\mathbf{Y}(n)) = \sqrt{\frac{1}{N-1}\sum_{i=2}^{N}\left(\hat{\mathbf{Y}}(n) - \frac{1}{N-1}\sum_{i=2}^{N}\mathbf{Y}(n)\right)^2}. \tag{35}$$

1000 independent simulations were performed to determine the average of the RAMSEs shown in the figures.

A. Estimation Accuracy

A key factor that would affect the performance of clock synchronization and relative positioning is the accuracy of parameter estimations. In this section, we present simulation results in the absence of any control signal. Fig. 5 shows how the RAMSEs varied as the number of communication cycles increased. To verify the proposed estimator in different dynamic scenarios, two case studies are presented. One case study is the scenario of long relative distance and high velocity, where the initial positions and velocities of the UAV members $\mathbf{P}_1$ and $\dot{\mathbf{P}}_1$ are arbitrarily chosen according to (36) and (37), respectively. For the other case study, to test the performance in the scenario of shorter distance and lower velocity, we set the positions and velocities to $\mathbf{P}_2 = 0.05\mathbf{P}_1$ and $\dot{\mathbf{P}}_2 = 0.1\dot{\mathbf{P}}_1$, respectively. We set the communication time interval $\Delta = 0.02$s.

$$\mathbf{P}_1 = \begin{bmatrix} 8958 & -1374 & -7 & 1935 & 38 \\ -13326 & 2890 & -3 & -699 & -1783 \\ 9683 & 11993 & 170 & 4248 & 3712 \end{bmatrix} \tag{36}$$

$$\dot{\mathbf{P}}_1 = \begin{bmatrix} 181 & -61 & -55 & 37 & -71 \\ -70 & 163 & 84 & -139 & 94 \\ 47 & 17 & -122 & -75 & -62 \end{bmatrix} \tag{37}$$

Figs. 5 and 6 show the performances of clock synchronization, ranging, and cooperative localization with respect to the communication cycles in two different scenarios. To understand the effect of choosing K for the RAMSE of the ranging and clock parameters, we investigated the performance of the proposed algorithm for $K = 1, 2, 3$. For the given experimental setup, optimality was achieved at $K = 2$, as shown in Fig. 5, although the performance of the estimators for $K = 3$ was similar. However, the estimator for $K = 3$ outperformed the estimator for $K = 2$, as shown in Fig. 6. Therefore, we can infer that selecting the optimal value of K depends on the motion states of UAV members. As expected, the proposed estimator exhibited the worst performance when the approximation order was $K = 1$ because the relative distance was always nonlinear even if the nodes moved in a

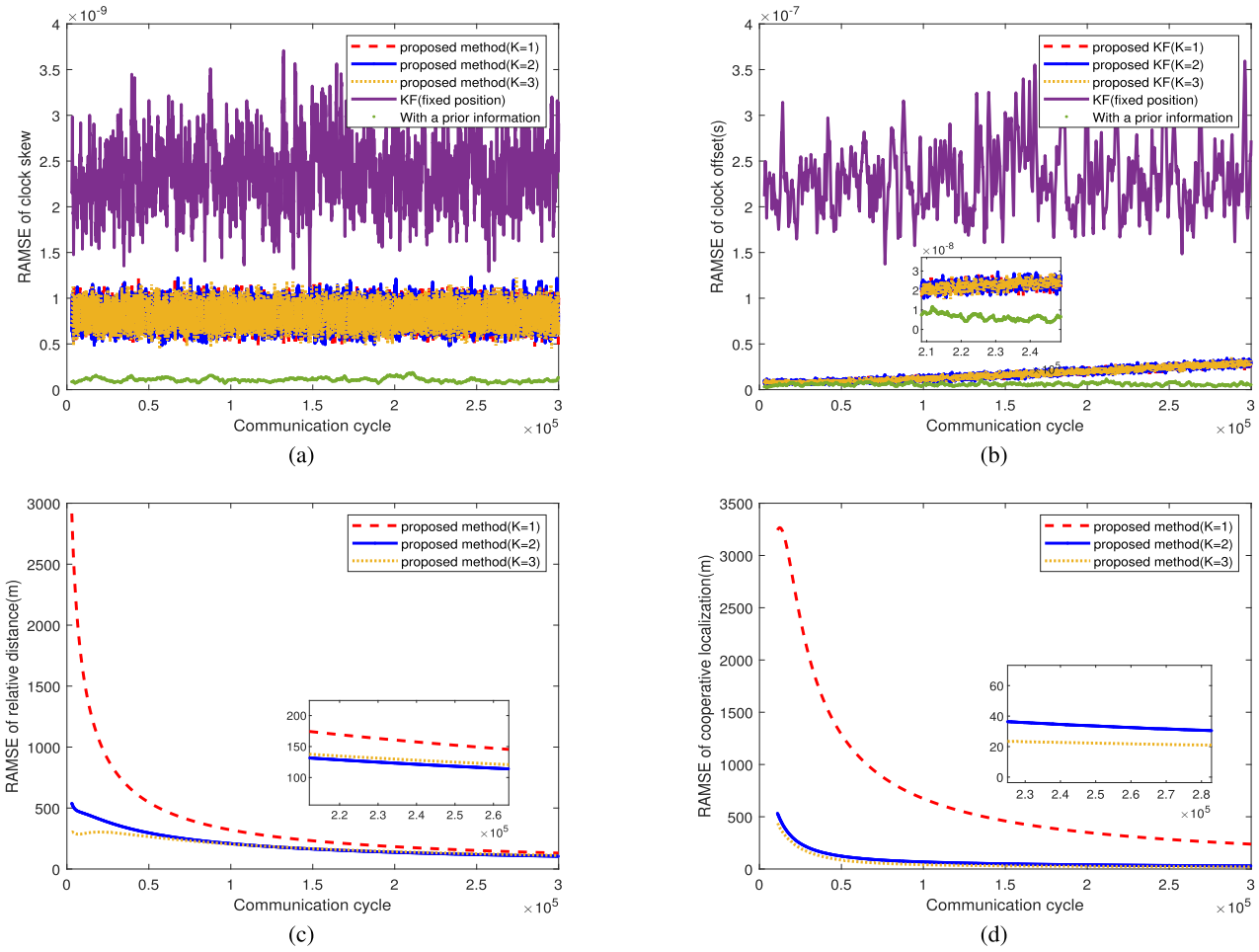

Fig. 6. RAMSEs for clock skew (a), clock offset (b), relative distance (c), and cooperative localization (d) with respect to the communication cycles in the scenario with initial positions $\mathbf{P}_1$ and velocities $\dot{\mathbf{P}}_1$.

straight line with a constant velocity. The convergence slopes shown in Figs. 5d and 5c are similar because the cooperative localization results were calculated using MDS in this study, whose accuracy relies on ranging measurements.

Furthermore, we can infer that the RAMSEs in Fig.5 are smaller than those in Fig. 6. This is because the approximation made in (14) becomes less accurate in the scenario of long distance and high velocity; that is, increasing the signal transmission delay degrades the approximation.

The simulation result labeled 'with prior information' indicates the KF-based estimator, which first used known positions and velocities to calculate $\chi_{ij}(n)$ and $\chi_{ij}(n)$ in (8) and (9) and then estimated clock skew $\boldsymbol{\omega}(n)$ and clock offset $\boldsymbol{\delta}(n)$. The estimator of prior information outperformed the other algorithms, which was expected because the error originating from the relative motion could be significantly decoupled when the prior information of positions and velocities was accurate. Unlike in satellite systems and networks with anchor nodes, the real-time positions and velocities of UAV members are difficult to determine in advance. Therefore, the degradation in accuracy is acceptable.

To present a comprehensive comparison, we added a KF estimator based on the conventional two-way ranging algorithm shown in Fig. 5b, which ignored the effect on the relative motion and assumed that the transmission delay of the forward link was equal to that of the reverse link. This method had a lower accuracy compared to the proposed estimator, which indicates that the proposed method is capable of effectively decoupling the clock parameters for the mobile network. However, similar to the results shown in Fig. 5a, the results for the different K values were also similar.

The RAMSEs of the proposed estimator for $K = 2$ are compared against varying communication time intervals in Fig. 7. The proposed estimator showed a considerable improvement over the conventional KF when estimating the clock parameters. Although Figs. 7c and 7d show that the RAMSEs of ranging and positioning are not proportional to the communication time interval, usually, clock steering leads to a more accurate physical clock synchronization performance.

B. Clock Adjustment

Physical time synchronization helps the system eliminate the subsequent errors originating from the UAV clocks. In this section, we consider the order of the Taylor series, $K = 2$. The clock of a member UAV was selected to represent stability before and after being steered by different control laws. Two types of clocks with different stabilities were compared, and the results are shown in Fig. 8. To demonstrate the superiority

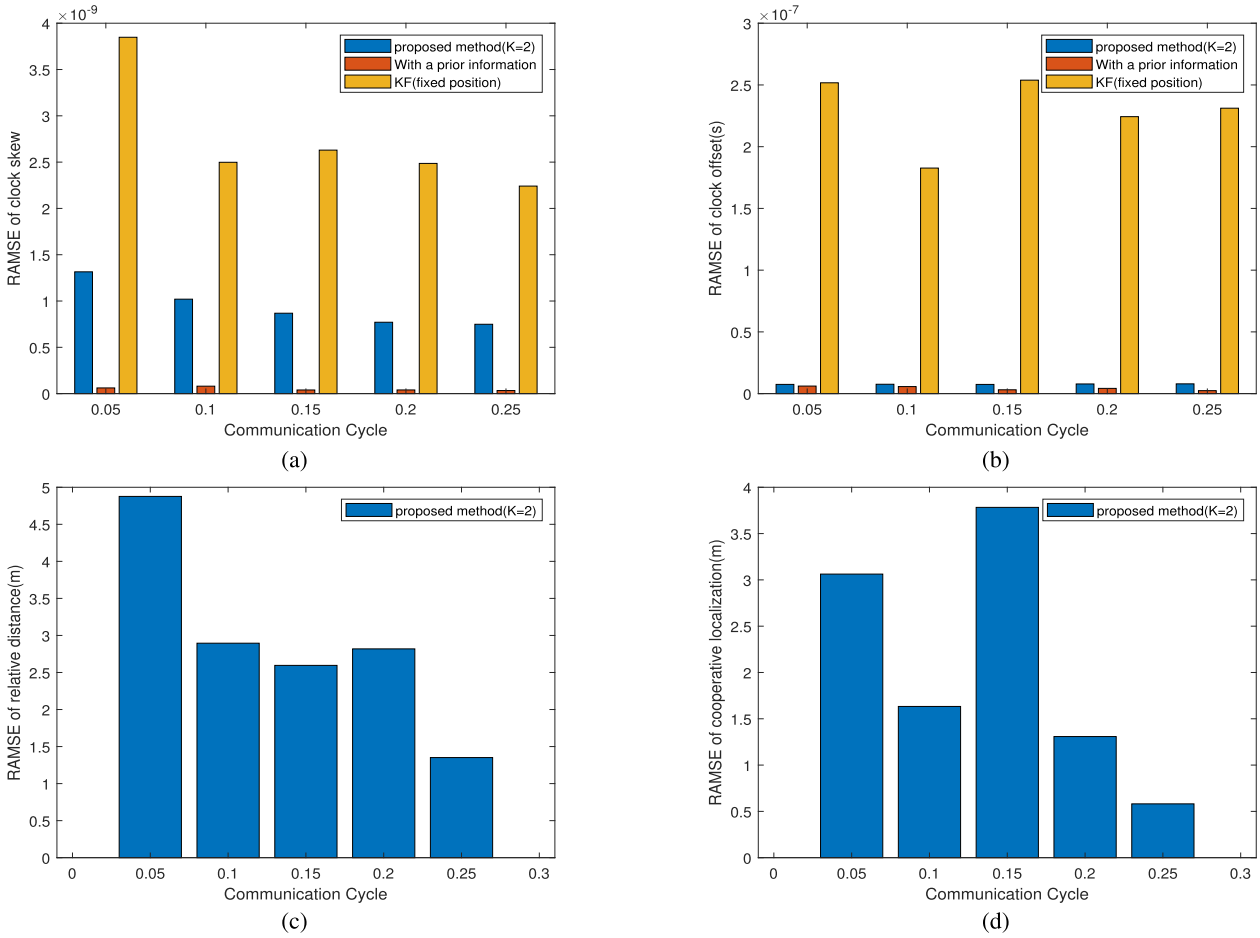

Fig. 7. RAMSEs for clock skew (a), clock offset (b), relative distance (c), and cooperative localization (d) with respect to varying communication time interval in the scenario with initial positions $\mathbf{P}_2$ and velocities $\dot{\mathbf{P}}_2$.

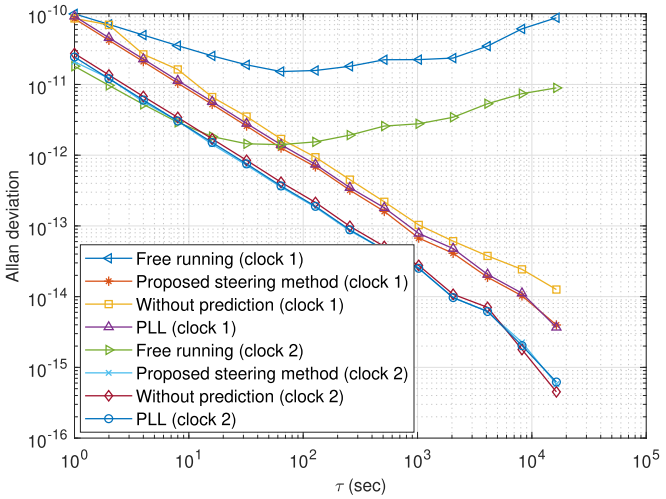

Fig. 8. Comparison of the Allan Deviations of the on-board clock steered by different control approaches.

of the proposed method, we present the control law, which starts to generate the control signal $\mathbf{\Lambda}(n)$ by $\hat{\mathbf{X}}(n-2)$ without a clock offset prediction, namely, the control signals of frequency and phase equal to $\hat{\boldsymbol{\omega}}(n-2)$ and $\hat{\boldsymbol{\delta}}(n-2)$ in this case. In addition, the simulation results of the steering approach using a 3^{rd}-order PLL are presented. All three clock adjustment methods improved the clock's stability. Compared with the method without prediction, the input of the controller, namely, the estimation accuracy of clock parameters for the upcoming clock adjustment time instant, determined the performance. Moreover, clock-steering approaches performed better on a less accurate clock, especially with respect to short-term stability. In particular, the proposed steering method slightly outperformed the 3^{rd}-order PLL for clock 1; however, the two methods had similar effects when steering clock 2.

These results provide a theoretical basis for clock selection, and thus the overall cost could be better controlled. Moreover, we can infer that after two rounds of two-way ranging, the member node could collect all pseudorange measurements to construct the EDM and generate the input signal.

VI. Conclusion

The problem of achieving high-precision clock synchronization, frequency syntonization, and ranging through rounds of two-way pseudorange measurements was addressed in this study. A practical KF-based parameter estimation method that does not require prior information or assistance from an external system is proposed. The estimator performs real-time onboard clock adjustments and ranges. The simulation results show that the synchronization precision is inversely proportional to the communication time interval because the precision of the Taylor series expression of the relative motion

strongly relies on the approximation time, and the clock adjustment should also be operated as fast as possible. Moreover, the clock adjustment algorithm can improve the stability of the onboard VCXO by remote steering using a reference clock; that is, the overall cost of the UAV system can be reduced via such a design.

The features of the proposed estimator imply that it can also be applied to other potential scenarios, such as deep-space engineering, UWSN, indoor positioning, robot systems, satellite networks, and cross-domain unmanned systems. Moreover, the proposed method can be integrated with other sensors such as GNSS receivers, inertial measurement units (IMUs), and visual navigation. Research on the accuracies of clock synchronization and cooperative localization, which can only be obtained by pseudorange measurements, can also better guide its integration with these sensors to further improve system performance. Promising future directions include applying a machine-learning-based approach to improve the estimation accuracy of the relative motion model and developing an adaptive estimation algorithm to optimally select the order of the fitted polynomial. In addition, when the EDM is corrupted owing to occlusion, insufficient communication radius, or strong electromagnetic interference, recovering it by using historical ranging data and the current rigid graph characteristics of the formation is also an interesting topic.

REFERENCES

[1] Q. Liu, R. Liu, Z. Wang, and J. S. Thompson, "UAV swarm-enabled localization in isolated region: A rigidity-constrained deployment perspective," *IEEE Wireless Commun. Lett.*, vol. 10, no. 9, pp. 2032–2036, Sep. 2021.

[2] M. U. de Haag, S. Huschbeck, and J. Huff, "SUAS swarm navigation using inertial, range radios and partial GNSS," in *Proc. IEEE/AIAA 38th Digit. Avionics Syst. Conf. (DASC)*, Sep. 2019, pp. 1–10.

[3] K. F. Hasan, Y. Feng, and Y.-C. Tian, "GNSS time synchronization in vehicular ad-hoc networks: Benefits and feasibility," *IEEE Trans. Intell. Transp. Syst.*, vol. 19, no. 12, pp. 3915–3924, Dec. 2018.

[4] T. Dass, G. Freed, J. Petzinger, J. Rajan, T. J. Lynch, and J. Vaccaro, "GPS clocks in space: Current performance and plans for the future," in *Proc. 34th Annu. Precise Time Time Interval Syst. Appl. Meeting*, Dec. 2002, pp. 175–192.

[5] X. Xie, T. Geng, Q. Zhao, Y. Lv, H. Cai, and J. Liu, "Orbit and clock analysis of BDS-3 satellites using inter-satellite link observations," *J. Geodesy*, vol. 94, no. 7, pp. 1–18, Jul. 2020.

[6] M. Vasile, F. Torre, R. Serra, and S. Grey, "Autonomous orbit determination and navigation for formations of CubeSats beyond LEO," in *Proc. 9th Int. Workshop Satell. Constellations Formation Flying*, 2017, pp. 1–20.

[7] B. Etzlinger, H. Wymeersch, and A. Springer, "Cooperative synchronization in wireless networks," *IEEE Trans. Signal Process.*, vol. 62, no. 11, pp. 2837–2849, Jun. 2014.

[8] Y.-C. Wu, Q. Chaudhari, and E. Serpedin, "Clock synchronization of wireless sensor networks," *IEEE Signal Process. Mag.*, vol. 28, no. 1, pp. 124–138, Jan. 2011.

[9] R. Chen, B. Yang, and W. Zhang, "Distributed and collaborative localization for swarming UAVs," *IEEE Internet Things J.*, vol. 8, no. 6, pp. 5062–5074, Mar. 2021.

[10] Z. Deng, H. Qi, C. Wu, E. Hu, and R. Wang, "A cluster positioning architecture and relative positioning algorithm based on pigeon flock bionics," *Satell. Navigat.*, vol. 4, no. 1, pp. 1–21, Dec. 2023.

[11] C.-S. Jao et al., "Sub-meter accurate pedestrian indoor navigation system with dual ZUPT-aided INS, machine learning-aided LTE, and UWB signals," in *Proc. Int. Tech. Meeting Satell. Division Inst. Navigat.*, Oct. 2022, pp. 1108–1126.

[12] X. Ouyang, F. Zeng, D. Lv, T. Dong, and H. Wang, "Cooperative navigation of UAVs in GNSS-denied area with colored RSSI measurements," *IEEE Sensors J.*, vol. 21, no. 2, pp. 2194–2210, Jan. 2021.

[13] S. Xu, L. Wu, K. Dogançay, and M. Alaee-Kerahroodi, "A hybrid approach to optimal TOA-sensor placement with fixed shared sensors for simultaneous multi-target localization," *IEEE Trans. Signal Process.*, vol. 70, pp. 1197–1212, 2022.

[14] S. Mazuelas, A. Conti, J. C. Allen, and M. Z. Win, "Soft range information for network localization," *IEEE Trans. Signal Process.*, vol. 66, no. 12, pp. 3155–3168, Jun. 2018.

[15] P. C. Ng, P. Spachos, J. She, and K. Plataniotis, "A kernel method to nonlinear location estimation with RSS-based fingerprint," *IEEE Trans. Mobile Comput.*, vol. 22, no. 8, pp. 4388–4404, Aug. 2023.

[16] E. D. Kaplan and C. Hegarty, *Understanding GPS/GNSS: Principles and Applications*. Norwood, MA, USA: Artech House, 2017.

[17] D. Van Buren, P. Axelrad, and S. Palo, "Design of a high-stability heterogeneous clock system for small satellites in LEO," *GPS Solutions*, vol. 25, no. 3, pp. 1–14, Jul. 2021.

[18] G. Zhang et al., "A method for precisely predicting satellite clock bias based on robust fitting of ARMA models," *GPS Solutions*, vol. 26, no. 1, pp. 1–15, Jan. 2022.

[19] J.-P. Montillet, G. W. Roberts, C. Hancock, X. Meng, O. Ogundipe, and J. Barnes, "Deploying a locata network to enable precise positioning in urban canyons," *J. Geodesy*, vol. 83, no. 2, pp. 91–103, Feb. 2009.

[20] S. Prager, M. S. Haynes, and M. Moghaddam, "Wireless subnanosecond RF synchronization for distributed ultrawideband software-defined radar networks," *IEEE Trans. Microw. Theory Techn.*, vol. 68, no. 11, pp. 4787–4804, Nov. 2020.

[21] M. Leng and Y.-C. Wu, "On clock synchronization algorithms for wireless sensor networks under unknown delay," *IEEE Trans. Veh. Technol.*, vol. 59, no. 1, pp. 182–190, Jan. 2010.

[22] K.-L. Noh, Q. M. Chaudhari, E. Serpedin, and B. W. Suter, "Novel clock phase offset and skew estimation using two-way timing message exchanges for wireless sensor networks," *IEEE Trans. Commun.*, vol. 55, no. 4, pp. 766–777, Apr. 2007.

[23] R. T. Rajan and A.-J. van der Veen, "Joint ranging and clock synchronization for a wireless network," in *Proc. 4th IEEE Int. Workshop Comput. Adv. Multi-Sensor Adapt. Process. (CAMSAP)*, Dec. 2011, pp. 297–300.

[24] X. Gu, J. Li, G. Zhou, and S. Xie, "Improved clock parameters tracking and ranging method based on two-way timing stamps exchange mechanism," *IEEE Signal Process. Lett.*, vol. 28, pp. 598–602, 2021.

[25] R. Wen, E. Schoof, and A. Chapman, "Clock rigidity and joint position-clock estimation in ultra-wideband sensor networks," *IEEE Trans. Control Netw. Syst.*, vol. 10, no. 3, pp. 1209–1221, Sep. 2023.

[26] R. M. Vaghefi and R. M. Buehrer, "Cooperative joint synchronization and localization in wireless sensor networks," *IEEE Trans. Signal Process.*, vol. 63, no. 14, pp. 3615–3627, Jul. 2015.

[27] Q. Shi, X. Cui, S. Zhao, S. Xu, and M. Lu, "BLAS: Broadcast relative localization and clock synchronization for dynamic dense multiagent systems," *IEEE Trans. Aerosp. Electron. Syst.*, vol. 56, no. 5, pp. 3822–3839, Oct. 2020.

[28] J. Liu, Z. Wang, J.-H. Cui, S. Zhou, and B. Yang, "A joint time synchronization and localization design for mobile underwater sensor networks," *IEEE Trans. Mobile Comput.*, vol. 15, no. 3, pp. 530–543, Mar. 2016.

[29] R. T. Rajan and A.-J. van der Veen, "Joint ranging and synchronization for an anchorless network of mobile nodes," *IEEE Trans. Signal Process.*, vol. 63, no. 8, pp. 1925–1940, Apr. 2015.

[30] J.-G. Park, E. D. Demaine, and S. Teller, "Moving-baseline localization," in *Proc. Int. Conf. Inf. Process. Sensor Netw. (IPSN)*, Apr. 2008, pp. 15–26.

[31] J. Zheng and Y.-C. Wu, "Joint time synchronization and localization of an unknown node in wireless sensor networks," *IEEE Trans. Signal Process.*, vol. 58, no. 3, pp. 1309–1320, Mar. 2010.

[32] T. Wang, H. Xiong, H. Ding, and L. Zheng, "TDOA-based joint synchronization and localization algorithm for asynchronous wireless sensor networks," *IEEE Trans. Commun.*, vol. 68, no. 5, pp. 3107–3124, May 2020.

[33] A. Ahmad, E. Serpedin, H. Nounou, and M. Nounou, "Joint node localization and time-varying clock synchronization in wireless sensor networks," *IEEE Trans. Wireless Commun.*, vol. 12, no. 10, pp. 5322–5333, Oct. 2013.

[34] X. Gu, G. Zhou, J. Li, and S. Xie, "Joint time synchronization and ranging for a mobile wireless network," *IEEE Commun. Lett.*, vol. 24, no. 10, pp. 2363–2366, Oct. 2020.

[35] M. Farina, L. Galleani, P. Tavella, and S. Bittanti, "A control theory approach to clock steering techniques," *IEEE Trans. Ultrason., Ferroelectr., Freq. Control*, vol. 57, no. 10, pp. 2257–2270, Oct. 2010.
[36] Y. S. Shmaliy, S. H. Khan, S. Zhao, and O. Ibarra-Manzano, "General unbiased FIR filter with applications to GPS-based steering of oscillator frequency," *IEEE Trans. Control Syst. Technol.*, vol. 25, no. 3, pp. 1141–1148, May 2017.
[37] W. Wang, S. Dong, W. Wu, D. Guo, X. Wang, and H. Song, "Combining TWSTFT and GPS PPP using a Kalman filter," *GPS Solutions*, vol. 25, no. 4, pp. 1–12, Oct. 2021.
[38] G. Giorgi and C. Narduzzi, "Performance analysis of Kalman-filter-based clock synchronization in IEEE 1588 networks," *IEEE Trans. Instrum. Meas.*, vol. 60, no. 8, pp. 2902–2909, Aug. 2011.
[39] B. Xue, Z. Li, P. Lei, Y. Wang, and X. Zou, "Wicsync: A wireless multi-node clock synchronization solution based on optimized UWB two-way clock synchronization protocol," *Measurement*, vol. 183, Oct. 2021, Art. no. 109760.
[40] L. Schenato and F. Fiorentin, "Average TimeSynch: A consensus-based protocol for clock synchronization in wireless sensor networks," *Automatica*, vol. 47, no. 9, pp. 1878–1886, Sep. 2011.
[41] R. Carli, A. Chiuso, L. Schenato, and S. Zampieri, "A PI consensus controller for networked clocks synchronization," *IFAC Proc. Volumes*, vol. 41, no. 2, pp. 10289–10294, 2008.
[42] Y. Xu, Q. Chang, and Z. Yu, "On new measurement and communication techniques of GNSS inter-satellite links," *Sci. China Technol. Sci.*, vol. 55, no. 1, pp. 285–294, Jan. 2012.
[43] C. Zucca and P. Tavella, "The clock model and its relationship with the Allan and related variances," *IEEE Trans. Ultrason., Ferroelectr., Freq. Control*, vol. 52, no. 2, pp. 289–296, Feb. 2005.
[44] X. Gu et al., "An autonomous satellite time synchronization system using remotely disciplined VC-OCXOs," *Sensors*, vol. 15, no. 8, pp. 17895–17915, Jul. 2015.
[45] E. Glennon, J. Gauthier, M. Choudhury, K. Parkinson, and A. G. Dempster, "Project Biarri and the NAMURU V3. 2 spaceborne GPS receiver," in *Proc. Int. Global Navigat. Satell. Syst. Soc., (IGNSS) Symp.*, 2013, pp. 1–11.

Xiaobo Gu received the B.Eng. and M.Sc. degrees from the University of Electronic Science and Technology of China, Chengdu, China, in 2008 and 2011, respectively, and the Ph.D. degree from Beihang University, Beijing, China, in 2016. From 2016 to 2018, he was the Director of the Power Dispatching and Control Center, China Southern Power Grid, Guangzhou. He is currently an Assistant Professor with the School of Automation, Guangdong University of Technology, Guangzhou, China. His current research interests include signal processing and communication systems, particularly synchronization and ranging and positioning techniques for wireless networks.

Chengye Zheng received the B.E. degree from the Mechanical and Electrical Engineering Department, Guangdong University of Technology, Guangzhou, China, in 2021, where he is currently pursuing the M.E. degree in electrical and information engineering. His current research interests include cooperative localization for wireless sensor networks.

Zeyu Li received the B.Sc. degree from Chang'an University, Xi'an, China, and the Ph.D. degree from the University of New South Wales, Sydney, Australia. He is currently a Lecturer of surveying engineering with the Shandong University of Science and Technology. Previously, he was an Engineer with Huawei Technologies Company Ltd., for the AR/VR products. His current research interests include multiple sensor-based localization, computer vision, and robotics. He serves as the Guest Editor for *Remote Sensing* and a reviewer for *Journal of Navigation* and *Acta Automatica Sinica*.

Guoxu Zhou (Member, IEEE) received the Ph.D. degree in intelligent signal and information processing from the South China University of Technology in 2010. He was a Research Scientist with the Brain Science Institute, Japan. He is currently a Full Professor and the Dean with the School of Automation, Guangdong University of Technology. He has authored more than 70 peer-reviewed articles that have been published in prestigious journals, such as PROCEEDINGS OF THE IEEE, *IEEE Signal Processing Magazine*, IEEE TRANSACTIONS ON SIGNAL PROCESSING, IEEE TRANSACTIONS ON NEURAL NETWORKS AND LEARNING SYSTEMS, IEEE TRANSACTIONS ON CYBERNETICS, and IEEE TRANSACTIONS ON IMAGE PROCESSING. His current research interests include tensor analysis, intelligent information processing, and artificial intelligence. He serves as an Associate Editor for IEEE TRANSACTIONS ON NEURAL NETWORKS AND LEARNING SYSTEMS and IEEE TRANSACTIONS ON SYSTEMS, MAN, AND CYBERNETICS: SYSTEMS.

Haibo Zhou (Senior Member, IEEE) received the Ph.D. degree in information and communication engineering from Shanghai Jiao Tong University, Shanghai, China, in 2014. From 2014 to 2017, he was a Post-Doctoral Fellow with the Broadband Communications Research Group, Department of Electrical and Computer Engineering, University of Waterloo. He is currently a Full Professor with the School of Electronic Science and Engineering, Nanjing University, Nanjing, China. His current research interests include resource management and protocol design in B5G/6G networks, vehicular ad hoc networks, and space-air-ground integrated networks. He was a recipient of the 2019 IEEE ComSoc Asia–Pacific Outstanding Young Researcher Award, the 2023–2024 IEEE ComSoc Distinguished Lecturer, and the 2023–2025 IEEE VTS Distinguished Lecturer. He served as the Track/Symposium Co-Chair for IEEE/CIC ICCC 2019, IEEE VTC-Fall 2020, IEEE VTC-Fall 2021, WCSP 2022, IEEE GLOBECOM 2022, and IEEE ICC 2024. He is currently an Associate Editor of IEEE TRANSACTIONS ON WIRELESS COMMUNICATIONS, IEEE INTERNET OF THINGS JOURNAL, *IEEE Network Magazine*, and *Journal of Communications and Information Networks*.

Lian Zhao (Senior Member, IEEE) received the Ph.D. degree from the Department of Electrical and Computer Engineering (ELCE), University of Waterloo, Canada, in 2002. She joined the Department of Electrical, Computer, and Biomedical Engineering, Toronto Metropolitan University (formerly Ryerson University), Toronto, Canada, in 2003, where she was a Professor in 2014. Her current research interests include wireless communications, radio resource management, mobile edge computing, caching and communications, and the Internet of Vehicles networks. She has been an IEEE Communication Society (ComSoc) and IEEE Vehicular Technology Society (VTS) Distinguished Lecturer (DL). She received the Best Land Transportation Paper Award from IEEE VTS in 2016, the Top 15 Editor in 2015 for IEEE TRANSACTION ON VEHICULAR TECHNOLOGY, the Best Paper Award from the 2013 International Conference on Wireless Communications and Signal Processing (WCSP), the Best Student Paper Award (with her student) from Chinacom in 2011, and the Canada Foundation for Innovation (CFI) New Opportunity Research Award in 2005. She served as the Co-General Chair for IEEE GreeenCom 2018, the Co-Chair for IEEE Globecom 2020 and IEEE ICC 2018 Wireless Communication Symposium, the Workshop Co-Chair for IEEE/CIC ICCC 2015, the Local Arrangement Co-Chair for IEEE VTC Fall 2017 and IEEE Infocom 2014, and the Co-Chair for IEEE Global Communications Conference (GLOBECOM) 2013 Communication Theory Symposium. She has been serving as an Editor for IEEE TRANSACTIONS ON VEHICULAR TECHNOLOGY, IEEE TRANSACTIONS ON WIRELESS COMMUNICATIONS, and IEEE INTERNET OF THINGS JOURNAL.